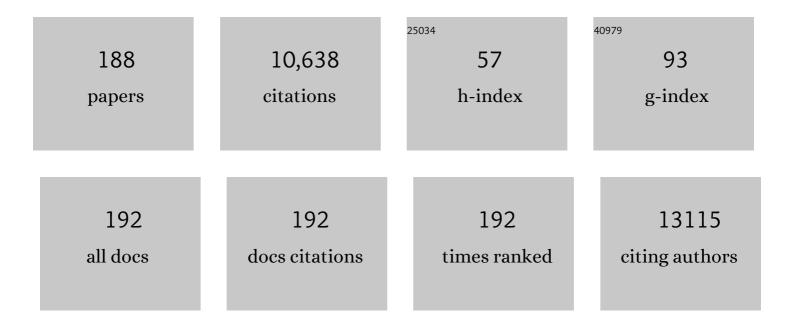
Guozhong Wang

List of Publications by Year in descending order

Source: https://exaly.com/author-pdf/3784299/publications.pdf Version: 2024-02-01



#	Article	IF	CITATIONS
1	Cobalt Covalent Doping in MoS ₂ to Induce Bifunctionality of Overall Water Splitting. Advanced Materials, 2018, 30, e1801450.	21.0	402
2	Potassiumâ€lonâ€Assisted Regeneration of Active Cyano Groups in Carbon Nitride Nanoribbons: Visibleâ€Lightâ€Driven Photocatalytic Nitrogen Reduction. Angewandte Chemie - International Edition, 2019, 58, 16644-16650.	13.8	356
3	Co/Co9S8@S,N-doped porous graphene sheets derived from S, N dual organic ligands assembled Co-MOFs as superior electrocatalysts for full water splitting in alkaline media. Nano Energy, 2016, 30, 93-102.	16.0	260
4	3D graphene/l̂´-MnO ₂ aerogels for highly efficient and reversible removal of heavy metal ions. Journal of Materials Chemistry A, 2016, 4, 1970-1979.	10.3	257
5	Bifunctional NH ₂ -MIL-88(Fe) metal–organic framework nanooctahedra for highly sensitive detection and efficient removal of arsenate in aqueous media. Journal of Materials Chemistry A, 2017, 5, 23794-23804.	10.3	230
6	Co/CoO nanoparticles immobilized on Co–N-doped carbon as trifunctional electrocatalysts for oxygen reduction, oxygen evolution and hydrogen evolution reactions. Chemical Communications, 2016, 52, 5946-5949.	4.1	221
7	Mass production of micro/nanostructured porous ZnO plates and their strong structurally enhanced and selective adsorption performance for environmental remediation. Journal of Materials Chemistry, 2010, 20, 8582.	6.7	216
8	Metal-organic framework derived nitrogen-doped porous carbon@graphene sandwich-like structured composites as bifunctional electrocatalysts for oxygen reduction and evolution reactions. Carbon, 2016, 106, 74-83.	10.3	206
9	One-step synthesis of cobalt-doped MoS ₂ nanosheets as bifunctional electrocatalysts for overall water splitting under both acidic and alkaline conditions. Chemical Communications, 2018, 54, 3859-3862.	4.1	196
10	The influence of biochar type on long-term stabilization for Cd and Cu in contaminated paddy soils. Journal of Hazardous Materials, 2016, 304, 40-48.	12.4	195
11	Biomass-derived N-doped porous carbon as electrode materials for Zn-air battery powered capacitive deionization. Chemical Engineering Journal, 2018, 334, 1270-1280.	12.7	182
12	Efficient Synthesis of Furfuryl Alcohol from H ₂ -Hydrogenation/Transfer Hydrogenation of Furfural Using Sulfonate Group Modified Cu Catalyst. ACS Sustainable Chemistry and Engineering, 2017, 5, 2172-2180.	6.7	177
13	Dramatically Enhanced Ambient Ammonia Electrosynthesis Performance by Inâ€Operando Created Li–S Interactions on MoS ₂ Electrocatalyst. Advanced Energy Materials, 2019, 9, 1803935.	19.5	176
14	Electrocatalytically Active Feâ€(Oâ€C ₂) ₄ Singleâ€Atom Sites for Efficient Reduction of Nitrogen to Ammonia. Angewandte Chemie - International Edition, 2020, 59, 13423-13429.	13.8	161
15	Synthesis and optical properties of S-doped ZnO nanowires. Applied Physics Letters, 2003, 82, 4791-4793.	3.3	154
16	Size Modulation of Zirconium-Based Metal Organic Frameworks for Highly Efficient Phosphate Remediation. ACS Applied Materials & Interfaces, 2017, 9, 32151-32160.	8.0	146
17	β-FeOOH Nanorods/Carbon Foam-Based Hierarchically Porous Monolith for Highly Effective Arsenic Removal. ACS Applied Materials & Interfaces, 2017, 9, 13480-13490.	8.0	143
18	Ambient Electrosynthesis of Ammonia on a Biomass-Derived Nitrogen-Doped Porous Carbon Electrocatalyst: Contribution of Pyridinic Nitrogen. ACS Energy Letters, 2019, 4, 377-383.	17.4	142

#	Article	IF	CITATIONS
19	NiFe-Layered Double Hydroxide Nanosheet Arrays Supported on Carbon Cloth for Highly Sensitive Detection of Nitrite. ACS Applied Materials & Interfaces, 2018, 10, 6541-6551.	8.0	140
20	Nitrogenâ€Doped Carbon Nanotube Confined Co–N <i>_x</i> Sites for Selective Hydrogenation of Biomassâ€Derived Compounds. Advanced Materials, 2019, 31, e1808341.	21.0	138
21	Cu doping in CeO ₂ to form multiple oxygen vacancies for dramatically enhanced ambient N ₂ reduction performance. Chemical Communications, 2019, 55, 2952-2955.	4.1	138
22	Facile fabrication of composition-tunable Fe/Mg bimetal-organic frameworks for exceptional arsenate removal. Chemical Engineering Journal, 2019, 357, 579-588.	12.7	124
23	Transforming chitosan into N-doped graphitic carbon electrocatalysts. Chemical Communications, 2015, 51, 1334-1337.	4.1	117
24	Fe/Fe2O3 nanoparticles anchored on Fe-N-doped carbon nanosheets as bifunctional oxygen electrocatalysts for rechargeable zinc-air batteries. Nano Research, 2016, 9, 2123-2137.	10.4	116
25	Simultaneously high-rate furfural hydrogenation and oxidation upgrading on nanostructured transition metal phosphides through electrocatalytic conversion at ambient conditions. Applied Catalysis B: Environmental, 2019, 244, 899-908.	20.2	115
26	Polyacrylonitrile/ferrous chloride composite porous nanofibers and their strong Cr-removal performance. Journal of Materials Chemistry, 2011, 21, 991-997.	6.7	108
27	S,N-Containing Co-MOF derived Co ₉ S ₈ @S,N-doped carbon materials as efficient oxygen electrocatalysts and supercapacitor electrode materials. Inorganic Chemistry Frontiers, 2017, 4, 491-498.	6.0	108
28	Hierarchical iron containing Î ³ -MnO 2 hollow microspheres: A facile one-step synthesis and effective removal of As(III) via oxidation and adsorption. Chemical Engineering Journal, 2016, 301, 139-148.	12.7	106
29	One-pot synthesis of nanotube-based hierarchical copper silicate hollow spheres. Chemical Communications, 2008, , 6555.	4.1	104
30	Micro/nanostructured α-Fe2O3 spheres: synthesis, characterization, and structurally enhanced visible-light photocatalytic activity. Journal of Materials Chemistry, 2012, 22, 9704.	6.7	103
31	Enhanced Gas-Sensing Properties of the Hierarchical TiO ₂ Hollow Microspheres with Exposed High-Energy {001} Crystal Facets. ACS Applied Materials & Interfaces, 2015, 7, 24902-24908.	8.0	99
32	Pseudocapacitive deionization of uranium(VI) with WO3/C electrode. Chemical Engineering Journal, 2020, 398, 125460.	12.7	99
33	Synthesis and photoluminescence properties of ZnMnS nanobelts. Applied Physics Letters, 2004, 84, 2157-2159.	3.3	98
34	Shrimp-shell derived carbon nanodots as carbon and nitrogen sources to fabricate three-dimensional N-doped porous carbon electrocatalysts for the oxygen reduction reaction. Physical Chemistry Chemical Physics, 2016, 18, 4095-4101.	2.8	97
35	Feâ€Co Alloyed Nanoparticles Catalyzing Efficient Hydrogenation of Cinnamaldehyde to Cinnamyl Alcohol in Water. Angewandte Chemie - International Edition, 2020, 59, 23521-23526.	13.8	91
36	Carbon-embedded Ni nanocatalysts derived from MOFs by a sacrificial template method for efficient hydrogenation of furfural to tetrahydrofurfuryl alcohol. Dalton Transactions, 2017, 46, 6358-6365.	3.3	88

#	Article	IF	CITATIONS
37	Formation of BNC Coordination to Stabilize the Exposed Active Nitrogen Atoms in gâ€C ₃ N ₄ for Dramatically Enhanced Photocatalytic Ammonia Synthesis Performance. Small, 2020, 16, e1906880.	10.0	88
38	In situ growth of α-Fe ₂ O ₃ nanorod arrays on 3D carbon foam as an efficient binder-free electrode for highly sensitive and specific determination of nitrite. Journal of Materials Chemistry A, 2017, 5, 4726-4736.	10.3	86
39	Hydrothermal synthesis and characterization of KNbO3 nanorods. CrystEngComm, 2009, 11, 1958.	2.6	84
40	Highly Ordered Single Crystalline Nanowire Array Assembled Three-Dimensional Nb ₃ O ₇ (OH) and Nb ₂ O ₅ Superstructures for Energy Storage and Conversion Applications. ACS Nano, 2016, 10, 507-514.	14.6	81
41	Highly selective liquid-phase hydrogenation of furfural over N-doped carbon supported metallic nickel catalyst under mild conditions. Molecular Catalysis, 2017, 429, 51-59.	2.0	81
42	Modified natural diatomite and its enhanced immobilization of lead, copper and cadmium in simulated contaminated soils. Journal of Hazardous Materials, 2015, 289, 210-218.	12.4	80
43	Nitrogen-free commercial carbon cloth with rich defects for electrocatalytic ammonia synthesis under ambient conditions. Chemical Communications, 2018, 54, 11188-11191.	4.1	79
44	Ethanol introduced synthesis of ultrastable 1T-MoS2 for removal of Cr(VI). Journal of Hazardous Materials, 2020, 394, 122525.	12.4	79
45	Two-dimensional CoNi nanoparticles@S,N-doped carbon composites derived from S,N-containing Co/Ni MOFs for high performance supercapacitors. Journal of Materials Chemistry A, 2017, 5, 9873-9881.	10.3	75
46	Effects of surface ligands on the uptake and transport of gold nanoparticles in rice and tomato. Journal of Hazardous Materials, 2016, 314, 188-196.	12.4	73
47	Zn nanobelts: a new quasi one-dimensional metal nanostructure. Chemical Communications, 2001, , 2632-2633.	4.1	71
48	High-Efficiency Co/Co _{<i>x</i>} S _{<i>y</i>} @S,N-Codoped Porous Carbon Electrocatalysts Fabricated from Controllably Grown Sulfur- and Nitrogen-Including Cobalt-Based MOFs for Rechargeable Zinc–Air Batteries. ACS Applied Materials & Interfaces, 2017, 9, 34269-34278.	8.0	71
49	Hierarchical Porous Carbon Materials Derived from Kelp for Superior Capacitive Applications. ACS Sustainable Chemistry and Engineering, 2019, 7, 8735-8743.	6.7	71
50	Co ₉ S ₈ @N,P-doped porous carbon electrocatalyst using biomass-derived carbon nanodots as a precursor for overall water splitting in alkaline media. RSC Advances, 2017, 7, 19181-19188.	3.6	69
51	Ambient Electrosynthesis of Ammonia on a Core–Shell‣tructured Au@CeO ₂ Catalyst: Contribution of Oxygen Vacancies in CeO ₂ . Chemistry - A European Journal, 2019, 25, 5904-5911.	3.3	69
52	Spontaneous Redox Approach to the Self-Assembly Synthesis of Au/CeO ₂ Plasmonic Photocatalysts with Rich Oxygen Vacancies for Selective Photocatalytic Conversion of Alcohols. ACS Applied Materials & Interfaces, 2018, 10, 31394-31403.	8.0	67
53	A fluorescent chitosan hydrogel detection platform for the sensitive and selective determination of trace mercury(<scp>ii</scp>) in water. Journal of Materials Chemistry A, 2015, 3, 19455-19460.	10.3	66
54	3D Fe ₃ O ₄ @Au@Ag nanoflowers assembled magnetoplasmonic chains for in situ SERS monitoring of plasmon-assisted catalytic reactions. Journal of Materials Chemistry A, 2016, 4, 8866-8874.	10.3	63

#	Article	IF	CITATIONS
55	Europium-based infinite coordination polymer nanospheres as an effective fluorescence probe for phosphate sensing. RSC Advances, 2017, 7, 8661-8669.	3.6	62
56	Vapour-phase hydrothermal synthesis of Ni2P nanocrystallines on carbon fiber cloth for high-efficiency H2 production and simultaneous urea decomposition. Electrochimica Acta, 2017, 254, 44-49.	5.2	62
57	Highly Dispersed Copper Nanoparticles Supported on Activated Carbon as an Efficient Catalyst for Selective Reduction of Vanillin. Small, 2018, 14, e1801953.	10.0	62
58	Fabrication of hierarchical iron-containing MnO ₂ hollow microspheres assembled by thickness-tunable nanosheets for efficient phosphate removal. Journal of Materials Chemistry A, 2016, 4, 14814-14826.	10.3	60
59	Selective Determination of Cr(VI) by Glutaraldehyde Cross-Linked Chitosan Polymer Fluorophores. ACS Sensors, 2018, 3, 792-798.	7.8	60
60	A hierarchical hybrid monolith: MoS ₄ ^{2â^'} -intercalated NiFe layered double hydroxide nanosheet arrays assembled on carbon foam for highly efficient heavy metal removal. Journal of Materials Chemistry A, 2019, 7, 12869-12881.	10.3	58
61	Vapor-phase hydrothermal growth of single crystalline NiS2 nanostructure film on carbon fiber cloth for electrocatalytic oxidation of alcohols to ketones and simultaneous H2 evolution. Nano Research, 2018, 11, 1004-1017.	10.4	56
62	Liberating N NTs Confined Highly Dispersed CoN <i>_x</i> Sites for Selective Hydrogenation of Quinolines. Advanced Materials, 2019, 31, e1906051.	21.0	56
63	Three-dimensional honeycomb-like structured zero-valent iron/chitosan composite foams for effective removal of inorganic arsenic in water. Journal of Colloid and Interface Science, 2016, 478, 421-429.	9.4	55
64	Ultrafine nickel–cobalt alloy nanoparticles incorporated into three-dimensional porous graphitic carbon as an electrode material for supercapacitors. Journal of Materials Chemistry A, 2016, 4, 17080-17086.	10.3	53
65	Enhanced removal of trace Cr(VI) from neutral and alkaline aqueous solution by FeCo bimetallic nanoparticles. Journal of Colloid and Interface Science, 2016, 472, 8-15.	9.4	51
66	Ni/carbon aerogels derived from water induced self-assembly of Ni-MOF for adsorption and catalytic conversion of oily wastewater. Chemical Engineering Journal, 2020, 402, 126205.	12.7	51
67	Enhanced fluoride removal by hierarchically porous carbon foam monolith with high loading of UiO-66. Journal of Colloid and Interface Science, 2019, 542, 269-280.	9.4	50
68	Preparation and characterization of ordered semiconductor CdO nanowire arrays. Journal of Materials Science Letters, 2001, 20, 1687-1689.	0.5	49
69	In situ self-assembly synthesis and photocatalytic performance of hierarchical Bi0.5Na0.5TiO3 micro/nanostructures. Journal of Materials Chemistry, 2009, 19, 2253.	6.7	49
70	Lignosulfonate functionalized g-C ₃ N ₄ /carbonized wood sponge for highly efficient heavy metal ion scavenging. Journal of Materials Chemistry A, 2020, 8, 12687-12698.	10.3	48
71	Highly dispersed Co and Ni nanoparticles encapsulated in N-doped carbon nanotubes as efficient catalysts for the reduction of unsaturated oxygen compounds in aqueous phase. Catalysis Science and Technology, 2018, 8, 5506-5514.	4.1	47
72	Vapor-phase hydrothermal transformation of a nanosheet array structure Ni(OH) ₂ into ultrathin Ni ₃ S ₂ nanosheets on nickel foam for high-efficiency overall water splitting. Journal of Materials Chemistry A, 2018, 6, 19201-19209.	10.3	47

#	Article	IF	CITATIONS
73	In Situ Synthesis of Highly Dispersed Cu–Co Bimetallic Nanoparticles for Tandem Hydrogenation/Rearrangement of Bioderived Furfural in Aqueous-Phase. ACS Sustainable Chemistry and Engineering, 2018, 6, 14919-14925.	6.7	46
74	Adsorption of Hg ²⁺ by thiol functionalized hollow mesoporous silica microspheres with magnetic cores. RSC Advances, 2015, 5, 51446-51453.	3.6	45
75	Micro/nanostructured porous Fe–Ni binary oxide and its enhanced arsenic adsorption performances. Journal of Colloid and Interface Science, 2015, 458, 94-102.	9.4	45
76	Fabrication of hierarchically porous NH2-MIL-53/wood-carbon hybrid membrane for highly effective and selective sequestration of Pb2+. Chemical Engineering Journal, 2020, 387, 124141.	12.7	44
77	Selective electrocatalytic hydrogenation of nitrobenzene over copper-platinum alloying catalysts: Experimental and theoretical studies. Applied Catalysis B: Environmental, 2021, 298, 120545.	20.2	44
78	An efficient and reusable bimetallic Ni3Fe NPs@C catalyst for selective hydrogenation of biomass-derived levulinic acid to γ-valerolactone. Chinese Journal of Catalysis, 2018, 39, 1599-1607.	14.0	43
79	Theoretical study of single transition metal atom modified MoP as a nitrogen reduction electrocatalyst. Physical Chemistry Chemical Physics, 2019, 21, 5950-5955.	2.8	43
80	Selective Pseudocapacitive Deionization of Calcium Ions in Copper Hexacyanoferrate. ACS Applied Materials & Interfaces, 2020, 12, 41437-41445.	8.0	43
81	Encapsulated Ni-Co alloy nanoparticles as efficient catalyst for hydrodeoxygenation of biomass derivatives in water. Chinese Journal of Catalysis, 2021, 42, 2027-2037.	14.0	43
82	Structure-enhanced removal of Cr(<scp>vi</scp>) in aqueous solutions using MoS ₂ ultrathin nanosheets. New Journal of Chemistry, 2018, 42, 9006-9015.	2.8	42
83	MoS ₂ Nanodots Anchored on Reduced Graphene Oxide for Efficient N ₂ Fixation to NH ₃ . ACS Sustainable Chemistry and Engineering, 2020, 8, 2320-2326.	6.7	42
84	One-step fabrication of high performance micro/nanostructured Fe3S4–C magnetic adsorbent with easy recovery and regeneration properties. CrystEngComm, 2013, 15, 2956.	2.6	40
85	Efficient electrochemical N ₂ fixation by doped-oxygen-induced phosphorus vacancy defects on copper phosphide nanosheets. Journal of Materials Chemistry A, 2020, 8, 5936-5942.	10.3	40
86	Enhanced photocatalytic activity of hierarchical structure TiO ₂ hollow spheres with reactive (001) facets for the removal of toxic heavy metal Cr(<scp>vi</scp>). RSC Advances, 2014, 4, 34577-34583.	3.6	39
87	Experimental and theoretical understanding on electrochemical activation and inactivation processes of Nb ₃ O ₇ (OH) for ambient electrosynthesis of NH ₃ . Journal of Materials Chemistry A, 2019, 7, 16969-16978.	10.3	39
88	Ambient Electrosynthesis of Ammonia Using Core–Shell Structured Au@C Catalyst Fabricated by One-Step Laser Ablation Technique. ACS Applied Materials & Interfaces, 2019, 11, 44186-44195.	8.0	38
89	Plasma-etching enhanced titanium oxynitride active phase with high oxygen content for ambient electrosynthesis of ammonia. Electrochemistry Communications, 2019, 100, 90-95.	4.7	38
90	Hierarchically porous poly(amidoxime)/bacterial cellulose composite aerogel for highly efficient scavenging of heavy metals. Journal of Colloid and Interface Science, 2021, 600, 752-763.	9.4	38

#	Article	IF	CITATIONS
91	Self-assembled Pd/CeO2 catalysts by a facile redox approach for high-efficiency hydrogenation of levulinic acid into gamma-valerolactone. Catalysis Communications, 2017, 93, 10-14.	3.3	37
92	Highly efficient removal of hexavalent chromium in aqueous solutions <i>via</i> chemical reduction of plate-like micro/nanostructured zero valent iron. RSC Advances, 2017, 7, 55905-55911.	3.6	37
93	Efficient electrocatalytic nitrogen reduction to ammonia with aqueous silver nanodots. Communications Chemistry, 2021, 4, .	4.5	36
94	Three-dimensional hierarchically structured PAN@γ–AlOOH fiber films based on a fiber templated hydrothermal route and their recyclable strong Cr(vi)-removal performance. RSC Advances, 2012, 2, 1769.	3.6	35
95	In Situ Growth of Ultrathin Ni(OH) ₂ Nanosheets as Catalyst for Electrocatalytic Oxidation Reactions. ChemSusChem, 2021, 14, 2935-2942.	6.8	35
96	Electrodeposition of hierarchically amorphous FeOOH nanosheets on carbonized bamboo as an efficient filter membrane for As(III) removal. Chemical Engineering Journal, 2020, 392, 123773.	12.7	34
97	A three-dimensional porous Co@C/carbon foam hybrid monolith for exceptional oil–water separation. Nanoscale, 2019, 11, 12161-12168.	5.6	33
98	Highly selective capacitive deionization of copper ions in FeS2@N, S co-doped carbon electrode from wastewater. Separation and Purification Technology, 2021, 262, 118336.	7.9	33
99	Highly efficient electrocatalytic oxidation of urea on a Mn-incorporated Ni(OH) ₂ /carbon fiber cloth for energy-saving rechargeable Zn–air batteries. Chemical Communications, 2017, 53, 10711-10714.	4.1	32
100	Orientable pore-size-distribution of ZnO nanostructures and their superior photocatalytic activity. CrystEngComm, 2010, 12, 2821.	2.6	31
101	Organization of Mn3O4nanoparticles into γ-MnOOHnanowiresvia hydrothermal treatment of the colloids induced by laser ablation in water. CrystEngComm, 2011, 13, 1063-1066.	2.6	31
102	Micro/nanostructured hydroxyapatite structurally enhances the immobilization for Cu and Cd in contaminated soil. Journal of Soils and Sediments, 2016, 16, 2030-2040.	3.0	31
103	Synthesis of KNbO ₃ Nanorods by Hydrothermal Method. Journal of Nanoscience and Nanotechnology, 2009, 9, 1465-1469.	0.9	29
104	Cobalt single atom catalysts for the efficient electrosynthesis of hydrogen peroxide. Inorganic Chemistry Frontiers, 2021, 8, 2829-2834.	6.0	29
105	Protein assisted hydrothermal synthesis of ultrafine magnetite nanoparticle built-porous oriented fibers and their structurally enhanced adsorption to toxic chemicals in solution. Journal of Materials Chemistry, 2011, 21, 11188.	6.7	28
106	Shrimp-shell derived carbon nanodots as precursors to fabricate Fe,N-doped porous graphitic carbon electrocatalysts for efficient oxygen reduction in zinc–air batteries. Inorganic Chemistry Frontiers, 2016, 3, 910-918.	6.0	27
107	Hollow mesoporous SiO ₂ sphere nanoarchitectures with encapsulated silver nanoparticles for catalytic reduction of 4-nitrophenol. Inorganic Chemistry Frontiers, 2016, 3, 663-670.	6.0	27
108	Electrocatalytic oxidation of benzyl alcohol for simultaneously promoting H ₂ evolution by a Co _{0.83} Ni _{0.17} /activated carbon electrocatalyst. New Journal of Chemistry, 2018, 42, 6381-6388.	2.8	27

#	Article	IF	CITATIONS
109	Porous carbon nanosheets functionalized with Fe ₃ O ₄ nanoparticles for capacitive removal of heavy metal ions from water. Environmental Science: Water Research and Technology, 2020, 6, 331-340.	2.4	27
110	Fe/Fe3C@CNTs anchored on carbonized wood as both self-standing anode and cathode for synergistic electro-Fenton oxidation and sequestration of As(III). Chemical Engineering Journal, 2021, 414, 128925.	12.7	27
111	Hierarchical Porous Iron Metal–Organic Gel/Bacterial Cellulose Aerogel: Ultrafast, Scalable, Room-Temperature Aqueous Synthesis, and Efficient Arsenate Removal. ACS Applied Materials & Interfaces, 2021, 13, 47684-47695.	8.0	27
112	Potassiumâ€lonâ€Assisted Regeneration of Active Cyano Groups in Carbon Nitride Nanoribbons: Visibleâ€Lightâ€Driven Photocatalytic Nitrogen Reduction. Angewandte Chemie, 2019, 131, 16797-16803.	2.0	26
113	Trimetallic Sulfide Hollow Superstructures with Engineered dâ€Band Center for Oxygen Reduction to Hydrogen Peroxide in Alkaline Solution. Advanced Science, 2022, 9, e2104768.	11.2	26
114	A facile synthesis of single crystal TiO2 nanorods with reactive {100} facets and their enhanced photocatalytic activity. CrystEngComm, 2014, 16, 3091.	2.6	25
115	Zirconium metal organic frameworks-based DGT technique for in situ measurement of dissolved reactive phosphorus in waters. Water Research, 2018, 147, 223-232.	11.3	24
116	An oxygen-coordinated molybdenum single atom catalyst for efficient electrosynthesis of ammonia. Chemical Communications, 2021, 57, 5410-5413.	4.1	24
117	A pyrolysis–phosphorization approach to fabricate carbon nanotubes with embedded CoP nanoparticles for ambient electrosynthesis of ammonia. Chemical Communications, 2019, 55, 12376-12379.	4.1	23
118	Electrocatalytically Active Feâ€(O ₂) ₄ Singleâ€Atom Sites for Efficient Reduction of Nitrogen to Ammonia. Angewandte Chemie, 2020, 132, 13525-13531.	2.0	23
119	A low-cost cementite (Fe ₃ C) nanocrystal@N-doped graphitic carbon electrocatalyst for efficient oxygen reduction. Physical Chemistry Chemical Physics, 2015, 17, 27527-27533.	2.8	22
120	Hydroxyapatite nanoparticles in root cells: reducing the mobility and toxicity of Pb in rice. Environmental Science: Nano, 2018, 5, 398-407.	4.3	22
121	Hollow carbon sphere encapsulated nickel nanoreactor for aqueous-phase hydrogenation-rearrangement tandem reaction with enhanced catalytic performance. Applied Catalysis B: Environmental, 2022, 306, 121140.	20.2	22
122	General in situ chemical etching synthesis of ZnO nanotips array. Applied Physics Letters, 2008, 93, 153110.	3.3	21
123	Water bath synthesis and enhanced photocatalytic performances of urchin-like micro/nanostructured α-FeOOH. Journal of Materials Research, 2015, 30, 1629-1638.	2.6	21
124	Converting eggplant biomass into multifunctional porous carbon electrodes for self-powered capacitive deionization. Environmental Science: Water Research and Technology, 2019, 5, 1054-1063.	2.4	21
125	Enhancement of the visible-light photocatalytic activity of CeO ₂ by chemisorbed oxygen in the selective oxidation of benzyl alcohol. New Journal of Chemistry, 2019, 43, 7355-7362.	2.8	21
126	Pseudocapacitive desalination via valence engineering with spindle-like manganese oxide/carbon composites. Nano Research, 2021, 14, 4878-4884.	10.4	21

#	Article	IF	CITATIONS
127	Decomposition and Crystallization of a Sol?Gel-Derived PbTiO3Precursor. Journal of the American Ceramic Society, 2007, 90, 2649-2652.	3.8	20
128	Intrinsic Pseudocapacitive Affinity in Manganese Spinel Ferrite Nanospheres for High-Performance Selective Capacitive Removal of Ca ²⁺ and Mg ²⁺ . ACS Applied Materials & Interfaces, 2021, 13, 38886-38896.	8.0	20
129	Growth and in situ transformation of TiO2 and HTiOF3 crystals on chitosan-polyvinyl alcohol co-polymer substrates under vapor phase hydrothermal conditions. Nano Research, 2016, 9, 745-754.	10.4	19
130	Determination of mercury in aquatic systems by DGT device using thiol-modified carbon nanoparticle suspension as the liquid binding phase. New Journal of Chemistry, 2017, 41, 10305-10311.	2.8	19
131	A sulfonate group functionalized active carbon-based Cu catalyst for electrochemical ammonia synthesis under ambient conditions. Inorganic Chemistry Frontiers, 2019, 6, 2832-2836.	6.0	19
132	Laser Irradiation in Liquid to Release Cobalt Single-Atom Sites for Efficient Electrocatalytic N2 Reduction. ACS Applied Energy Materials, 2020, 3, 6079-6086.	5.1	19
133	Robust enhanced hydrogen production at acidic conditions over molybdenum oxides-stabilized ultrafine palladium electrocatalysts. Nano Research, 2021, 14, 268-274.	10.4	19
134	Highly sensitive detection of nitrite by using gold nanoparticle-decorated α-Fe ₂ O ₃ nanorod arrays as self-supporting photo-electrodes. Inorganic Chemistry Frontiers, 2019, 6, 1432-1441.	6.0	18
135	Converting Co2+-impregnated g-C3N4 into N-doped CNTs-confined Co nanoparticles for efficient hydrogenation rearrangement reactions of furanic aldehydes. Nano Research, 2021, 14, 2846-2852.	10.4	18
136	An adsorption–reduction synergistic effect of mesoporous Fe/SiO ₂ –NH ₂ hollow spheres for the removal of Cr(<scp>vi</scp>) ions. RSC Advances, 2016, 6, 27039-27046.	3.6	17
137	One-pot redox synthesis of Pt/Fe ₃ O ₄ catalyst for efficiently chemoselective hydrogenation of cinnamaldehyde. RSC Advances, 2017, 7, 21107-21113.	3.6	17
138	Efficiently electrocatalytic oxidation of benzyl alcohol for energy- saved zinc-air battery using a multifunctional nickel–cobalt alloy electrocatalyst. Journal of Colloid and Interface Science, 2018, 532, 37-46.	9.4	17
139	Highly dispersed nickel anchored on a N-doped carbon molecular sieve derived from metal–organic frameworks for efficient hydrodeoxygenation in the aqueous phase. Chemical Communications, 2020, 56, 6696-6699.	4.1	17
140	Tunable synthesis of imines and secondary-amines from tandem hydrogenation-coupling of aromatic nitro and aldehyde over NiCo5 bi-metallic catalyst. Applied Catalysis B: Environmental, 2021, 280, 119448.	20.2	17
141	Synchronous removal of tetracycline and water hardness ions by capacitive deionization. Journal of Cleaner Production, 2021, 316, 128251.	9.3	17
142	Synthesis of Carbon Materials–TiO ₂ Hybrid Nanostructures and Their Visibleâ€Light Photoâ€catalytic Activity. ChemPlusChem, 2014, 79, 454-461.	2.8	16
143	Magnetically recyclable catalytic activity of spiky magneto-plasmonic nanoparticles. RSC Advances, 2015, 5, 56653-56657.	3.6	16
144	Electrochemical deposition of Pt on carbon fiber cloth utilizing Pt mesh counter electrode during hydrogen evolution reaction for electrocatalytic hydrogenation reduction of p-nitrophenol. New Journal of Chemistry, 2017, 41, 7012-7019.	2.8	16

#	Article	IF	CITATIONS
145	Direct Conversion of Biomass into Compact Air Electrode with Atomically Dispersed Oxygen and Nitrogen Coordinated Copper Species for Flexible Zinc–Air Batteries. ACS Applied Energy Materials, 2019, 2, 8659-8666.	5.1	16
146	Selective Growth of Highâ€Density Anatase {101} Twin Boundaries on Highâ€Energy {001} Facets. Small Structures, 2020, 1, 2000025.	12.0	16
147	Improved Photocatalytic Performance of the Ultraâ€small Ag Nanocrystalliteâ€Decorated TiO ₂ Hollow Sphere Heterostructures. ChemCatChem, 2014, 6, 1392-1400.	3.7	15
148	Photoelectrochemical manifestation of intrinsic photoelectron transport properties of vertically aligned {001} faceted single crystal TiO ₂ nanosheet films. RSC Advances, 2015, 5, 55438-55444.	3.6	15
149	A nanoparticulate liquid binding phase based DCT device for aquatic arsenic measurement. Talanta, 2016, 160, 225-232.	5.5	15
150	Metal (Co/Mo)–N bond anchor-doped N in porous carbon for electrochemical nitrogen reduction. Inorganic Chemistry Frontiers, 2021, 8, 1476-1481.	6.0	15
151	Sustainable 2,5-furandicarboxylic synthesis by a direct 5-hydroxymethylfurfural fuel cell based on a bifunctional PtNiS _x catalyst. Chemical Communications, 2020, 56, 13611-13614.	4.1	15
152	Ambient Electrochemical Nitrogen Fixation over a Bifunctional Mo–(O–C ₂) ₄ Site Catalyst. Journal of Physical Chemistry C, 2022, 126, 965-973.	3.1	15
153	Simultaneous Separation and Recovery of Gold and Copper from Electronic Waste Enabled by an Asymmetric Electrochemical System. ACS Applied Materials & Interfaces, 2022, 14, 9544-9556.	8.0	15
154	Standing porous ZnO nanoplate-built hollow microspheres and kinetically controlled dissolution/crystal growth mechanism. Journal of Materials Research, 2012, 27, 951-958.	2.6	14
155	Efficient Synthesis of 2-Methylfuran from Bio-Derived Furfural over Supported Copper Catalyst: The Synergistic Effect of CuO _x and Cu. ChemistrySelect, 2017, 2, 9984-9991.	1.5	14
156	Improving the utilization rate of foliar nitrogen fertilizers by surface roughness engineering of silica spheres. Environmental Science: Nano, 2020, 7, 3526-3535.	4.3	14
157	Bacterial cellulose hybrid membrane grafted with high ratio of adipic dihydrazide for highly efficient and selective recovery of gold from e-waste. Separation and Purification Technology, 2022, 292, 121021.	7.9	14
158	Integration of Fe2O3-based photoanode and atomically dispersed cobalt cathode for efficient photoelectrochemical NH3 synthesis. Chinese Chemical Letters, 2021, 32, 805-810.	9.0	13
159	Enhanced photocatalytic activity of a hollow TiO ₂ –Au–TiO ₂ sandwich structured nanocomposite. RSC Advances, 2016, 6, 18958-18964.	3.6	12
160	Synergistic catalysis of cluster and atomic copper induced by copper-silica interface in transfer-hydrogenation. Nano Research, 2021, 14, 4601-4609.	10.4	12
161	Hierarchical Nanostructures of PbTiO ₃ Through Mesocrystal Formation. Journal of Nanoscience and Nanotechnology, 2007, 7, 2538-2541.	0.9	10
162	Threeâ€Ðimensional Nâ€doped Porous Carbon Derived from Monosodium Glutamate for Capacitive Deionization and the Oxygen Reduction Reaction. ChemElectroChem, 2018, 5, 3873-3880.	3.4	10

#	Article	IF	CITATIONS
163	The electrochemical corrosion of an air thermally-treated carbon fiber cloth electrocatalyst with outstanding oxygen evolution activity under alkaline conditions. Chemical Communications, 2019, 55, 2344-2347.	4.1	10
164	CoO _x @Co Nanoparticleâ€based Catalyst for Efficient Selective Transfer Hydrogenation of α,βâ€Unsaturated Aldehydes. ChemCatChem, 2020, 12, 1019-1024.	3.7	10
165	Rational Design of Cobaltâ€Platinum Alloy Decorated Cobalt Nanoparticles for Oneâ€Pot Synthesis of Imines from Nitroarenes and Aldehydes. ChemCatChem, 2020, 12, 5948-5958.	3.7	10
166	<i>In situ</i> transformation of Fe-doped Ni ₁₂ P ₅ into low-crystallized NiFe ₂ O ₄ with high-spin Fe ⁴⁺ for efficient electrocatalytic water oxidation. Journal of Materials Chemistry A, 2021, 9, 10289-10296.	10.3	10
167	Crystal plane effect of ceria on supported copper catalyst for liquid-phase hydrogenation of unsaturated aldehyde. Journal of Colloid and Interface Science, 2021, 596, 34-43.	9.4	10
168	The catalytic behaviour in aqueous-phase hydrogenation over a renewable Ni catalyst derived from a perovskite-type oxide. Dalton Transactions, 2018, 47, 17276-17284.	3.3	9
169	A universal route to fabricate bacterial cellulose-based composite membranes for simultaneous removal of multiple pollutants. Chemical Communications, 2021, 57, 8592-8595.	4.1	9
170	Facile synthesis of N, P co-doped carbon encapsulated Ni catalyst for green production of cyclopentanone from biomass derivative furfural. Fuel, 2022, 319, 123815.	6.4	9
171	Novel Fe ₃ O ₄ nanoparticles-based DGT device for dissolved reactive phosphate measurement. New Journal of Chemistry, 2018, 42, 2874-2881.	2.8	8
172	Iron covalent doping in WB ₂ to boost its hydrogen evolution activity. Inorganic Chemistry Frontiers, 2022, 9, 524-530.	6.0	8
173	Oxoacetohydrazideâ€functionalized cellulose with enhanced adsorption performance. Journal of Applied Polymer Science, 2016, 133, .	2.6	7
174	Co2P Nanoparticles Wrapped in Amorphous Porous Carbon as an Efficient and Stable Catalyst for Water Oxidation. Frontiers in Chemistry, 2018, 6, 580.	3.6	6
175	Monodispersed Zerovalent Iron Nanoparticles Decorated Carbon Submicrospheres for Enhanced Removal of DDT from Aqueous Solutions. ChemistrySelect, 2019, 4, 12134-12142.	1.5	6
176	Highly ordered Nb2O5 nanochannel film with rich oxygen vacancies for electrocatalytic N2 reduction: Inactivation and regeneration of electrode. Chinese Chemical Letters, 2021, 32, 2833-2836.	9.0	6
177	<i>In situ</i> growth of MOFs on Ni(OH) ₂ for efficient electrocatalytic oxidation of 5-hydroxymethylfurfural. Chemical Communications, 2021, 57, 11358-11361.	4.1	6
178	One pot microwave-assisted synthesis of Ag decorated yolk@shell structured TiO2 microspheres. RSC Advances, 2015, 5, 11349-11357.	3.6	5
179	Ball Milling-Induced Plate-like Sub-microstructured Iron for Enhancing Degradation of DDT in a Real Soil Environment. ACS Omega, 2018, 3, 6955-6961.	3.5	5
180	Copper nanocrystals anchored on an O-rich carbonized corn gel for nitrogen electroreduction to ammonia. Inorganic Chemistry Frontiers, 2020, 7, 3555-3560.	6.0	5

#	Article	IF	CITATIONS
181	Metalâ€Organic Frameworks Derived Titanium Oxides via Soft Interface Adaptive Transformation. Advanced Functional Materials, 2021, 31, 2107260.	14.9	5
182	hcp-phased Ni nanoparticles with generic catalytic hydrogenation activities toward different functional groups. Science China Materials, 2022, 65, 1252-1261.	6.3	5
183	A freestanding, hierarchically porous poly(imine dioxime) membrane enabling selective gold recovery from eâ€waste with unprecedented capacity. EcoMat, 2022, 4, .	11.9	5
184	Photocatalytic degradation of 2,4,4′-trichlorobiphenyl into long-chain alkanes using Ag nanoparticle decorated flower-like ZnO microspheres. New Journal of Chemistry, 2015, 39, 7781-7785.	2.8	4
185	Carbothermal Methods: Highly Dispersed Copper Nanoparticles Supported on Activated Carbon as an Efficient Catalyst for Selective Reduction of Vanillin (Small 36/2018). Small, 2018, 14, 1870164.	10.0	4
186	The Sorption of Sulfamethoxazole by Aliphatic and Aromatic Carbons from Lignocellulose Pyrolysis. Agronomy, 2022, 12, 476.	3.0	2
187	A combustion method to synthesize nanoporous graphene. RSC Advances, 2018, 8, 9320-9326.	3.6	1
188	Fe o Alloyed Nanoparticles Catalyzing Efficient Hydrogenation of Cinnamaldehyde to Cinnamyl Alcohol in Water. Angewandte Chemie, 2020, 132, 23727-23732.	2.0	1